Dalton Transactions

Cite this: *Dalton Trans.*, 2011, **40**, 10907

www.rsc.org/dalton

PAPER

Synthesis and characterization of diiron dithiolate complexes containing a quinoxaline bridge†

Fenfen Xu,[a,c] Shaowu Du,*[a] Yuping Liu,[b] Jacqueline Hassan,[b] Jie Zhang*[b] and Alan M. Bond*[b]

Received 21st May 2011, Accepted 15th July 2011
DOI: 10.1039/c1dt10953g

A potential model complex for the hydrogenase active site, $[Fe_2\{(\mu\text{-}CH_2S)_2R\}(CO)_6]$ (**1**) (R = quinoxaline), was synthesized by condensation of $[(\mu\text{-}LiS)_2Fe_2(CO)_6]$ with 2,3-bis(bromomethyl)-quinoxaline. Reactions of **1** with bis(diphenylphosphino)methane (dppm) under a range of conditions yielded substituted complexes $[Fe_2\{(\mu\text{-}CH_2S)_2R\}(CO)_5(dppm)]$ (**2**), $[Fe_2\{(\mu\text{-}CH_2S)_2R\}(CO)_4(k^2\text{-}dppm)]$ (**3**) and $[Fe_2\{(\mu\text{-}CH_2S)_2R\}(CO)_4(\mu\text{-}dppm)]$ (**4**). X-ray crystallography confirms that in **2**, the dppm is terminally bonded to an iron atom *via* one phosphorus atom, whereas in **3**, it acts as a chelating ligand to coordinate to an iron center in a dibasal-substituted manner. In **4**, the dppm bridges the two iron atoms in a *cis* basal/basal fashion with one phosphorus bonded to each iron atom. Treatment of **1** with various tertiary phosphines at room temperature in acetonitrile (MeCN) generates a range of mono-substituted products $[Fe_2\{(\mu\text{-}CH_2S)_2R\}(CO)_5L]$ (**5**, L = PEt_3; **6**, PMe_3; **7**, PPh_3; **8**, Me_2PPh). With Bu^tNC, mono- and di-substituted $[Fe_2\{(\mu\text{-}CH_2S)_2R\}(CO)_5(Bu^tNC)]$ (**9**) and $[Fe_2\{(\mu\text{-}CH_2S)_2R\}(CO)_4(Bu^tNC)_2]$ (**10**) complexes are generated. All the complexes were characterized by elemental analysis, IR, MS and NMR spectroscopy. IR and NMR spectroscopic studies suggest that addition of excess $HBF_4{\cdot}OEt_2$ acid to **1–4** led to the protonation of quinoxaline nitrogen atoms. In contrast, **5–10** were not stable in acidic media. Electrochemistry of **1–4** was investigated in the acetonitrile medium (0.1 M Bu_4NPF_6). The electrochemical instability of the reduced ligand, quinoxaline, and the reduced forms of these complexes revealed from the electrochemical studies suggests that they do not provide ideal models of the hydrogenase active site.

Introduction

Hydrogenases are a class of natural enzymes that can catalyse reversible and rapid hydrogen oxidation and evolution in many microorganisms.[1–4,7] Among them, [FeFe]-hydrogenases have been under intense investigations because of the unusual structures of their active sites and their extremely high capability for the production of "clean" and highly efficient hydrogen fuel.[4–6] X-Ray crystallographic studies on [FeFe]-hydrogenases isolated from *Clostridium pasteurianum* and *Desulfovibrio desulfuricans* have revealed that the active site is composed of a 2Fe2S butterfly structure (H-cluster), which is linked to an Fe_4S_4 cubane-like subcluster by a cysteine-S residue, and a three-atom linker ($-CH_2XCH_2-$, X = CH_2, NH or NH_2^+) bridged between the two S atoms of the 2Fe2S unit.[7–9] In order to mimic the behavior of metal–sulfur sites in hydrogenase, extensive research has been devoted to studies concerning synthetic models of the [FeFe]-hydrogenases by either CO substitution or bridge variation based on the well-known diiron complex $[Fe_2(\mu\text{-pdt})(CO)_6]$ (pdt = propane-1,3-dithiolato) with low overpotential and high efficiency towards hydrogen evolution reaction.[10–19] In contrast to the CO substitution, the variations of the S-to-S bridge linkers of the model complexes have received less attention. In the past few years, much effort has been focused on the functionalized azadithiolate Fe-only hydrogenases, $[Fe_2\{\mu\text{-}(SCH_2)_2NR\}(CO)_6]$, where the R groups range from alkyl,[16,20–25] aryl,[26–31] or heterocyclic substituents.[32–35] The N atoms in these model complexes can be protonated, leading to the reduction of the electron-donating capacity of the ligand, which may subsequently affect the electron density at the appended diiron site. Such effects upon protonation on N atoms may on one hand lead to positive shift in the reversible potentials of iron centers, thus lower the overpotential for hydrogen evolution, due to the introduction of positive charge, and on the other hand, provide a low energy pathway for molecular hydrogen production *via* proton–hydride combination.[28,32,36]

The overpotential of hydrogen evolution reaction also can be reduced by the introduction of unsaturated bridging motifs with electron-withdrawing character to the model complexes,

[a]*State Key Laboratory of Structural Chemistry, Fujian Institute of Research on the Structure of Matter, Chinese Academy of Sciences, Fuzhou, Fujian, 350002, P. R. China. E-mail: swdu@fjirsm.ac.cn; Fax: +86 591 83709470; Tel: +86 591 83709470*
[b]*School of Chemistry, Monash University, Clayton, Vic, 3800, Australia. E-mail: Jie.zhang@monash.edu, alan.bond@monash.edu; Fax: +61 3 99054597; Tel: +61 3 99056289,+61 3 99051338*
[c]*Graduate University of Chinese Academy of Sciences, Beijing, 100039, P. R. China*

† CCDC reference numbers 816112–816119. For crystallographic data in CIF or other electronic format see DOI: 10.1039/c1dt10953g

$[Fe_2(\mu\text{-}S_2R)(CO)_6]$ (S_2R = hydroquinone-2,3-dithiolate, 3,6-dichloro-1,2-benzenedithiolate, quinoxaline-2,3-dithiolate and 1,2-*closo*-$C_2B_{10}H_{10}$-1,2-dithiolate).[37–39] Among these model complexes, [Fe$_2$(μ-quinoxaline-2,3-dithiolate)(CO)$_6$] briefly reported by Ott and co-workers[38] is of particular interest since the N sites of quinoxaline may be protonated leading to the advantages associated with the $[Fe_2\{\mu\text{-}(SCH_2)_2NR\}(CO)_6]$ complexes mentioned above.[16,20,22–35]

Herein, we report the synthesis, and the spectroscopic and crystallographic characterization of a new diiron complex $[Fe_2\{(\mu\text{-}CH_2S)_2R\}(CO)_6]$ (**1**) (R = quinoxaline) and its derivatives which contain the rigid, conjugated, N atom containing an electron withdrawing quinoxaline group. We also describe the electrochemical studies employed to assess whether the new compounds could mimic the behaviors of hydrogenase.

Results and discussion

Synthesis and characterization of the model compound and its derivatives

The parent complex **1** was prepared by treatment of $[(\mu\text{-}S_2)Fe_2(CO)_6]$ with 2 equiv. of $LiBEt_3H$ in THF at –78 °C, followed by addition of 2,3-bis(bromomethyl)quinoxaline (Scheme 1). Column chromatography using petroleum ether and ethyl acetate (v/v: 6/1) as the eluents gave **1** as the major product. The infrared spectrum of **1** exhibits three absorption bands between 2079–2003 cm^{-1} that can be attributed to terminal carbonyl ligands. The ^{1}H NMR spectrum of **1** shows two doublets at 3.40 and 4.29 ppm (J_{HH} = 12.8 Hz) that can be assigned to the resonances of two methylene groups in the bismethylenequinoxaline linker. The inequivalence of the two protons on each methylene group could be due to the presence of bulky quinoxaline moiety which hinders the interconversion of the FeS(1)C(7)C(9)C(10)C(8)S(2) dithiacycloheptane ring (Fig. 1(a)), as observed in $[Fe_2\{\mu\text{-}(SCH_2)_2CHCOOH\}(CO)_6]$, in which the dithiacyclohexane ring carries a carboxylic substituent.[40]

The substitution of **1** with dppm in the presence of Me_3NO afforded different products depending on the reaction conditions employed (Scheme 2). When the reaction was carried out in acetonitrile (MeCN) at room temperature, complex **2**, where the ligand is monodentate, was isolated as the only product. Extension of the reaction time or addition of more CO scavenger did not give other products. However, when the reaction was performed in refluxing toluene, in addition to a small amount of **2**, two other products were both obtained in moderate

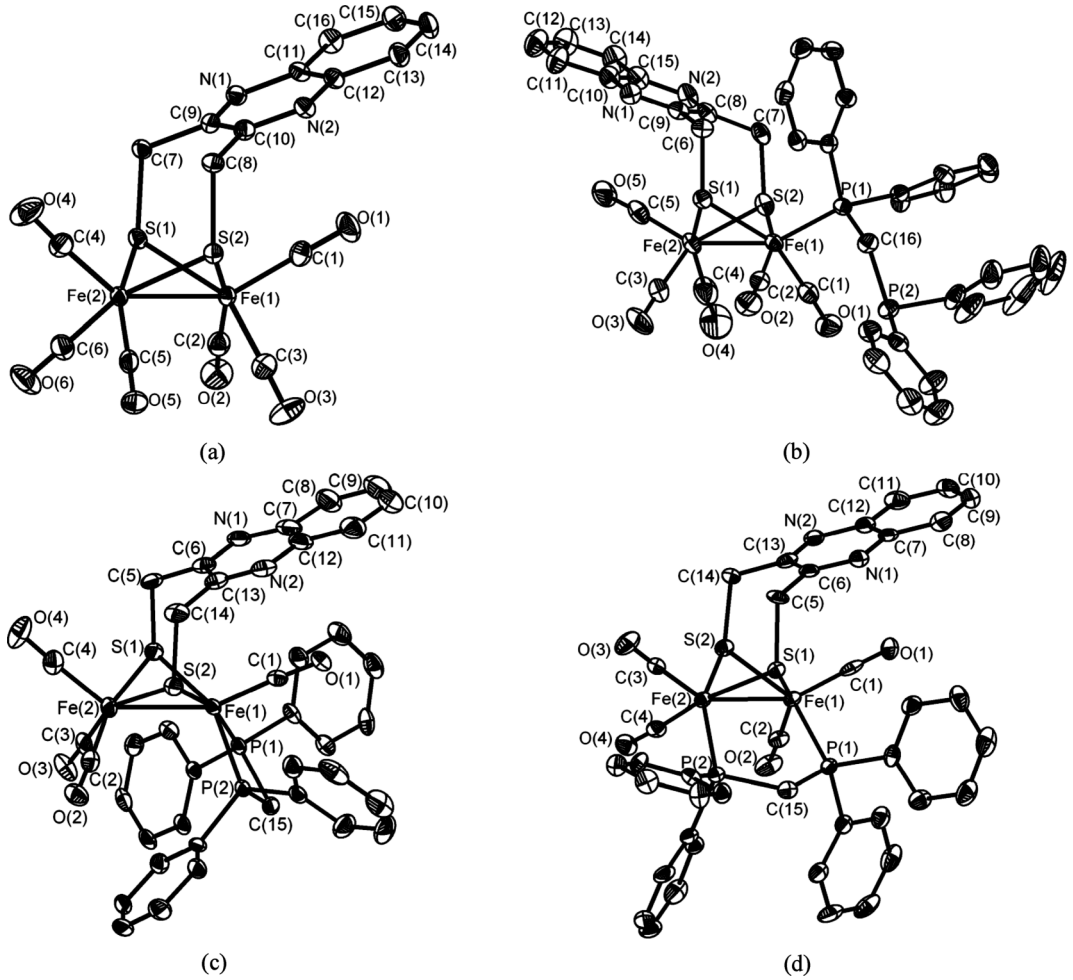

Fig. 1 Molecular structures of **1** (a), **2** (b), **3** (c) and **4** (d) with thermal ellipsoid set at 50% probability. The hydrogen atoms are omitted for clarity. The labels for C atoms of benzene rings are not shown for clarity.

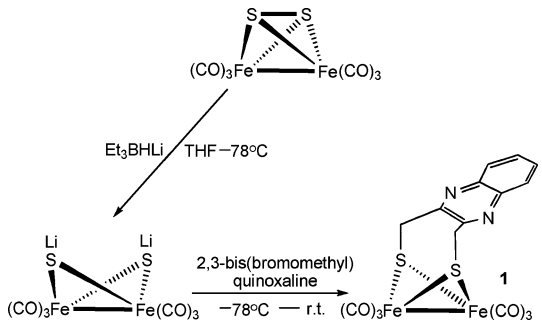

Scheme 1

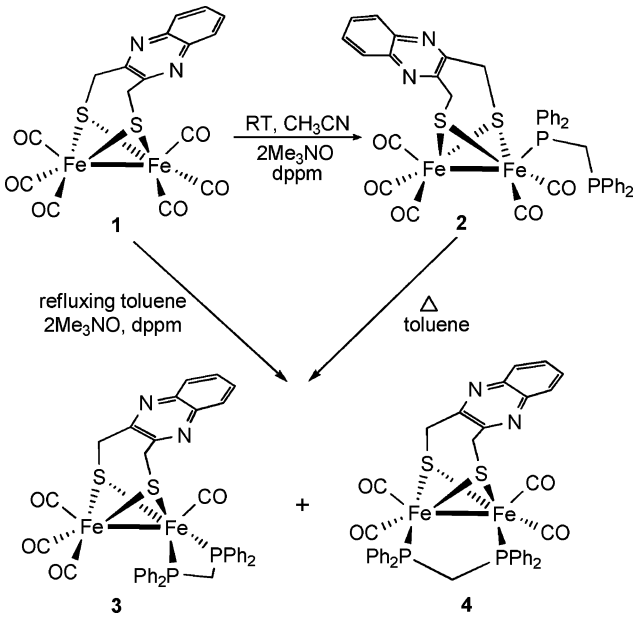

Scheme 2

yields. They were characterized as the dppm-chelated complex $[Fe_2\{(\mu\text{-}CH_2S)_2R\}(CO)_4(k^2\text{-dppm})]$ (**3**) and dppm-bridged complex $[Fe_2\{(\mu\text{-}CH_2S)_2R\}(CO)_4(\mu\text{-dppm})]$ (**4**). Compounds **3** and **4** can also be prepared by heating **2** in toluene. This indicates that **2** may be the intermediate for the formation of **3** and **4**. Complexes **2–4** each show three infrared bands in the ν(CO) stretching region (1916–2052 cm^{-1}). These substantial red-shifts of the ν(CO) bands compared to those of parent complexes reflect the increase of electron density of Fe atoms in complexes **2–4** which implies that **2–4** may be harder to reduce than complex **1**, but have a higher affinity to proton. In the ^{31}P NMR spectrum of **2**, a doublet for the coordinated P is found at 55.83 ppm, and a doublet for the uncoordinated phosphorus is found at –26.43 ppm. Complex **3** has diagnostic ^{31}P NMR signals at 8.44 and 12.43 ppm, and is different from $[Fe_2(\mu\text{-pdt})(CO)_4(k^2\text{-dppm})]$ reported by Adam *et al.*[41] where only one ^{31}P NMR signal was found for the chelated dppm ligand because of the fast flipping of the central methylene at room temperature which makes the two P atoms equivalent. The slight inequivalence of the two phosphorus atoms in **3** is most likely due to the fixed position of quinoxaline unit rather than the existence of apical-basal and dibasal isomers that normally display a difference in ^{31}P NMR chemical shifts about 10 ppm to each other.[42] This is in accordance with the observation of two resonances at 3.48 and 4.24 ppm associated with the methylene protons in the ^1H NMR spectrum. A similar situation was also observed for **4** whose ^{31}P NMR spectrum exhibits two very closely spaced doublets at δ = 52.42 and 54.08 ppm, indicating the existence of two slightly inequivalent P atoms.

Mono-substitution reactions of **1** with tertiary phosphines PR_3 were carried out according to literature procedures (Scheme 3). These reactions can be controlled at the mono-substituted stage at room temperature in MeCN with the aid of Me_3NO, resulting in the formation of a series of complexes $[Fe_2\{(\mu\text{-}CH_2S)_2R\}(CO)_5L]$ (**5**, L = PEt_3; **6**, PMe_3; **7**, PPh_3; **8**, PMe_2Ph). Similar to the dppm derivatives (complexes **2–4**), CO bands of complexes **5–8** in the IR spectra also shift to lower energy (2051–1926 cm^{-1}) compared to those of **1**, displaying the increase of electron density at the metal centers which again suggests that complexes **5–8** may be harder to reduce, but have higher proton affinity. However, variation in phosphine ligands appears to have a smaller influence on the shift of the ν(CO) bands of **5–8**. Their ^1H NMR spectra show the methylene protons as two doublets or singlets in the region of 3.35 to 4.46 ppm, thus again revealing the inequivalence of the two protons in each methylene group. As expected, their ^{31}P NMR spectra feature two resonance signals that are very close to each other, and are similar to those found in **2–4**.

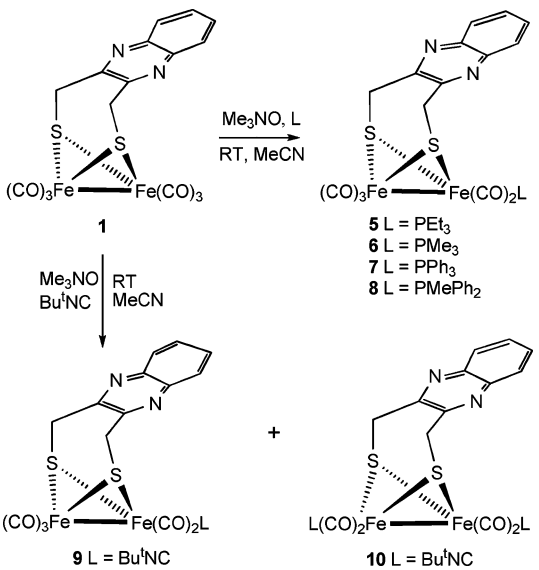

Scheme 3

Crystal structures of complexes 1–5, 7, 9 and 10

The molecular structures of **1–5**, **7**, **9** and **10** were established by X-ray crystallography. The molecular structures of **6** and **8** could not be obtained since attempts to obtain single crystals of these complexes were not successful. The ORTEP plots of complexes whose X-Ray structures could be obtained are presented in Fig. 1 and 2 and selected bond lengths and angles are tabulated in Table 1. As shown in Fig. 1 and 2, all the complexes contain a butterfly 2Fe2S core and a quinoxaline-2, 3-diyldimethanethiolate tether, which acts as a bidentate bridging ligand across the metal–metal bond and donates six electrons to make these complexes a 34 electron valance saturated bimetallic compound. Each iron center in all these complexes displays approximately square-pyramidal coordination geometry. The average Fe–Fe distance

Table 1 Selected bond lengths (Å) and angles (degrees) for **1–5**, **7**, **9** and **10**

1			
Fe(1)–S(1)	2.2587(11)	Fe(2)–S(1)	2.2569(12)
Fe(1)–S(2)	2.2598(11)	Fe(2)–S(2)	2.2604(12)
Fe(1)–C(1)	1.804(4)	Fe(2)–C(4)	1.798(4)
Fe(1)–C(2)	1.798(4)	Fe(2)–C(5)	1.804(4)
Fe(1)–C(3)	1.799(4)	Fe(2)–C(6)	1.797(4)
S(1)–Fe(1)–S(2)	88.02(4)	Fe(2)–S(1)–Fe(1)	67.88(3)
S(1)–Fe(2)–S(2)	88.05(4)	Fe(1)–S(2)–Fe(2)	67.80(3)
2			
Fe(1)–S(1)	2.2668(8)	Fe(2)–S(2)	2.2619(8)
Fe(1)–S(2)	2.2706(8)	Fe(1)–P(1)	2.2284(8)
Fe(2)–S(1)	2.2819(8)	Fe(1)–C(1)	1.779(3)
Fe(1)–C(2)	1.771(3)	Fe(2)–C(4)	1.789(4)
Fe(2)–C(3)	1.786(4)	Fe(2)–C(5)	1.810(4)
S(1)–Fe(2)–S(2)	86.57(3)	S(1)–Fe(1)–S(2)	86.72(3)
Fe(2)–S(2)–Fe(1)	67.12(3)	Fe(1)–S(1)–Fe(2)	66.85(2)
3			
Fe(1)–S(1)	2.2373(16)	Fe(2)–S(2)	2.2712(18)
Fe(1)–S(2)	2.2243(14)	Fe(1)–P(1)	2.2142(14)
Fe(2)–S(1)	2.2658(16)	Fe(1)–P(2)	2.2121(17)
Fe(1)–C(1)	1.751(5)	Fe(2)–C(3)	1.801(5)
Fe(2)–C(2)	1.780(5)	Fe(2)–C(4)	1.810(5)
S(1)–Fe(1)–S(2)	88.90(6)	P(2)–Fe(1)–S(1)	152.33(5)
S(1)–Fe(2)–S(2)	87.05(6)	P(2)–Fe(1)–S(2)	96.87(6)
P(1)–Fe(1)–P(2)	74.57(6)	Fe(1)–S(1)–Fe(2)	70.07(5)
P(1)–Fe(1)–S(1)	93.41(6)	Fe(1)–S(2)–Fe(2)	70.19(5)
P(1)–Fe(1)–S(2)	165.18(5)		
4			
Fe(1)–S(1)	2.2675(18)	Fe(2)–S(2)	2.2416(18)
Fe(1)–S(2)	2.252(2)	Fe(1)–P(1)	2.2025(19)
Fe(2)–S(1)	2.252(2)	Fe(2)–P(2)	2.2311(17)
Fe(1)–C(1)	1.787(7)	Fe(2)–C(3)	1.764(6)
Fe(1)–C(2)	1.774(6)	Fe(2)–C(4)	1.774(7)
S(1)–Fe(1)–S(2)	86.84(7)	Fe(1)–S(1)–Fe(2)	67.43(5)
S(1)–Fe(2)–S(2)	87.49(6)	Fe(1)–S(2)–Fe(2)	67.86(5)
5			
Fe(1)–S(1)	2.2652(15)	Fe(2)–S(2)	2.2591(16)
Fe(1)–S(2)	2.2426(14)	Fe(1)–P	2.2436(16)
Fe(2)–S(1)	2.2709(16)	Fe(1)–C(1)	1.765(5)
Fe(1)–C(2)	1.781(5)	Fe(2)–C(3)	1.796(5)
Fe(2)–C(4)	1.795(5)	Fe(2)–C(5)	1.800(5)
S(1)–Fe(1)–S(2)	87.92(6)	P–Fe(1)–S(2)	90.28(6)
S(2)–Fe(2)–S(1)	87.39(5)	Fe(1)–S(1)–Fe(2)	68.56(5)
P–Fe(1)–S(1)	168.08(5)	Fe(1)–S(2)–Fe(2)	69.15(4)
7			
Fe(1)–S(1)	2.2805(7)	Fe(2)–S(2)	2.2847(7)
Fe(1)–S(2)	2.2735(7)	Fe(1)–P	2.2441(7)
Fe(2)–S(1)	2.2679(7)	Fe(1)–C(1)	1.777(3)
Fe(1)–C(2)	1.773(3)	Fe(2)–C(3)	1.786(3)
Fe(2)–C(4)	1.785(3)	Fe(2)–C(5)	1.812(3)
S(1)–Fe(1)–S(2)	86.52(2)	P–Fe(1)–S(2)	107.38(3)
S(2)–Fe(1)–S(1)	86.52(2)	Fe(1)–S(1)–Fe(2)	67.13(2)
P–Fe(1)–S(1)	108.47(3)	Fe(1)–S(2)–Fe(2)	66.96(2)
9			
Fe(1)–S(1)	2.2447(13)	Fe(2)–S(2)	2.2648(14)
Fe(1)–S(2)	2.2632(13)	Fe(1)–C(16)	1.873(4)
Fe(2)–S(1)	2.2679(15)	N(3)–C(16)	1.160(5)
Fe(1)–C(1)	1.793(4)	Fe(2)–C(3)	1.791(5)
Fe(1)–C(2)	1.773(4)	Fe(2)–C(4)	1.790(5)
Fe(2)–C(5)	1.808(4)	Fe(1)–S(2)–Fe(2)	67.76(4)
S(1)–Fe(1)–S(2)	88.24(5)	C(16)–Fe(1)–S(1)	155.41(12)
S(1)–Fe(2)–S(2)	87.64(4)	C(16)–Fe(1)–S(2)	85.60(12)
Fe(1)–S(1)–Fe(2)	68.02(4)	C(16)–N(3)–C(17)	174.9(4)
10			
Fe(1)–S(1)	2.2646(10)	Fe(2)–C(20)	1.886(4)
Fe(1)–S(2)	2.2707(10)	N(3)–C(15)	1.149(4)
Fe(2)–S(1)	2.2756(10)	N(3)–C(16)	1.451(4)
Fe(2)–S(2)	2.2701(11)	N(4)–C(20)	1.151(4)
Fe(1)–C(15)	1.867(3)	N(4)–C(21)	1.463(4)
Fe(1)–C(1)	1.788(4)	Fe(2)–C(3)	1.786(4)
Fe(1)–C(2)	1.770(4)	Fe(2)–C(4)	1.780(4)
S(1)–Fe(1)–S(2)	87.67(4)	Fe(1)–S(2)–Fe(2)	66.87(3)
S(1)–Fe(2)–S(2)	87.42(3)	C(20)–Fe(2)–S(2)	100.64(11)
C(15)–Fe(1)–S(1)	154.60(11)	C(20)–Fe(2)–S(1)	101.91(10)
C(15)–Fe(1)–S(2)	83.09(11)	C(15)–N(3)–C(16)	177.0(3)
Fe(1)–S(1)–Fe(2)	66.88(3)	C(20)–N(4)–C(21)	177.7(4)

of these complexes (2.527 Å) is similar to the values reported for diiron dithiolate model complexes but slightly longer than those bearing rigid S-to-S linkers, such as [Fe_2(μ-bdt)$(CO)_6$] (2.480(2) Å),[43] [Fe_2{μ-$S_2C_6H_2(OH)_2$}$(CO)_6$] (2.4815(4) Å) [37] and [Fe_2(μ-Mebdt)$(CO)_6$] (2.4754(14) Å) [44] (bdt = benzene-1,2-dithiolato; Mebdt = 3,4-toluenedithiolate). Particularly noteworthy is that the Fe–Fe distance of **3** (2.5851(17) Å) is very close to those found in the structures of Fe-only hydrogenases (*ca.* 2.62 Å).[3] In the large number of previously reported 2Fe2S model complexes, few have Fe–Fe bond lengths larger than 2.58 Å. Examples reported so far include [Fe_2{(μ-*o*-xyldt)}$(CO)_4(PMe_3)_2$] (2.5825 Å)[42] and [Fe_2{(μ-$SCH_2)_2NBu^t$}$(CO)_5(I_{Mes})$] (2.5860 Å)[45] (*o*-xyldt = $SCH_2C_6H_4CH_2S$; I_{Mes} = 1,3-bis(mesityl)imidazole-2-ylidene). The mean bridging Fe–S distances are 2.2243(14)–2.2848(7) Å and the average Fe–S–Fe and S–Fe–S angles lie in the narrow range of 66.85(2)–70.19(5)° and 81.41(6)–88.90(6)°, respectively. The small variations in bond lengths and angles in this series of complexes indicate that the bonding characteristics of the 2Fe2S skeleton of parent complex **1** are slightly affected upon substitution of CO by other donor ligands. The average Fe–C(CO) and C–O bond lengths (1.787 and 1.145 Å, respectively) and Fe–C–O angles (178°) are as expected for these types of complexes. For each mono-substituted complex, the distances between the substituted iron atom and its attached CO-carbon atoms are shorter than those around the unsubstituted iron atom and reveals the increased strength of back-bonding from Fe to CO caused by coordination of the strong σ-donor ligand. For example, in **2**, **5** and **7**, the average Fe–C distances of phosphine-substituted Fe atoms is 1.775, 1.773 and 1.775 Å, which are shorter by *ca.* 0.02 Å respectively than those of their corresponding unsubstituted Fe atoms. This Fe–C bond shortening becomes particularly significant in the dppm chelated complex **3**, where the mean Fe–C bond length of substituted Fe is 0.05 Å shorter than that of the unsubstituted one.

In contrast to **2**, where one of the phosphorus atoms of dppm is coordinated to the Fe(1) center and the other is uncoordinated, in **3**, both the phosphorus atoms occupy basal sites and chelate to the Fe(1) atom. While there are a number of examples of dppm acting in a chelating manner bridging two iron atoms in hydrogenase model complexes, this dibasal geometry of dppm seems uncommon as this adoption requires a significant decrease in normal dibasal angle for iron center and P–C–P angle for dppm. The only crystallographically characterized example of this dibasal type model complex is in [Fe_2(μ-pdt)$(CO)_4$(k^2-dppm)].[41] The bite angle P(1)–Fe(1)–P(2) of **3** is 74.57(6)°, which is very small but comparable with the value found in [Fe_2(μ-pdt)$(CO)_4$(k^2-dppm)]. For complex **4**, the dppm bridges the two iron atoms with one P atom bonded to each iron atom and is *cis* to Fe–Fe bond. Unlike in **3** where the two Fe–P bond lengths are essentially equal, the Fe(1)–P(1) distance (2.2025 Å) is slightly shorter than that of Fe(2)–P(2) (2.2311 Å) in **4**. The P–C–P angle is 113.1°, very close to that of **2** with a different coordination mode.

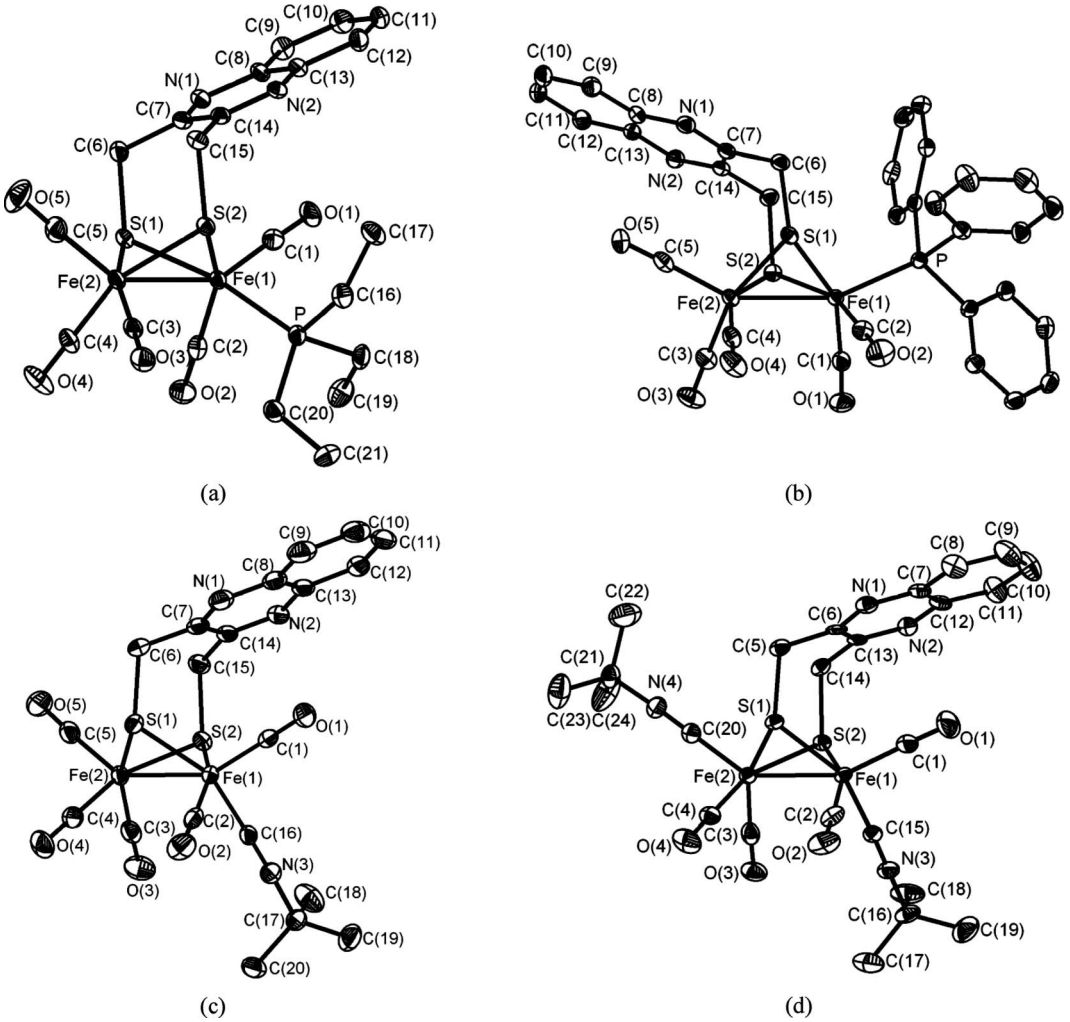

Fig. 2 Molecular structures of **5** (a), **7** (b), **9** (c) and **10** (d) with thermal ellipsoid set at 50% probability. The hydrogen atoms are omitted for clarity. The labels for C atoms of benzene rings are not shown for clarity.

It has been reported that there are four possible coordination configurations for double-CO displacement by two identical non-carbonyl ligands on each iron atom of several model complexes, which are, ap/ap, ap/ba, ba/ba (*trans*) and ba/ba (*cis*) configurations. For the doubly substituted complex **10**, one isocyanide occupies at the apical position while the other at the basal position (Fig. 2(d)). Such ap/ba arrangement is different from those in related complexes $[Fe_2(\mu\text{-pdt})(CO)_4(Bu^tNC)_2]$[12] and $[Fe_2\{(\mu\text{-}SCH_2)_2N(4\text{-}CH_3C_6H_4)\}(CO)_4(4\text{-}IC_6H_4NC)_2]$,[46] which have the isocyanide ligands in the ap/ap (*trans*) and ba/ba (*cis*) conformations in the solid state structure, respectively. The C–N–C angles of the *t*-Butylisocyanide in **10** [177.7(4)] and 177.0(3)°, respectively] are relatively linear, whereas that of **9** [174.9(4)°] is slightly bent.

A comparison of Fe–Fe bond lengths of these complexes shows that the metal–metal distance in the diiron compounds is slightly affected by the substitution position and the nature of the terminal ligands with a better electron-donating ability. For the mono-substituted complexes, substitution by an electron-donor ligand at the basal position leads to the elongation of Fe–Fe bond distance, whereas at the apical position it causes the decrease of the Fe–Fe bond lengths. For example, in comparison to the parent complex **1**, the Fe–Fe bond length of **5** is apparently longer by *ca*. 0.034 Å, while that of **2** shows slight decrease of 0.016 Å upon coordination of dppm to Fe(1). Complex **7** with PPh_3 lying in the apical position only shows a little decrease in Fe–Fe distance, which is in contrast to $[Fe_2(\mu\text{-Mebdt})(CO)_5(PPh_3)]$, where the axial PPh_3 causes the elongation of Fe–Fe bond.[44] In comparison with **1**, the Fe–Fe bond length in **3** shows significant lengthening by 0.064 Å, whereas in **4**, it shortens by 0.013 Å. This could be due to their different coordination manners of dppm ligands.

In the mono-substituted complexes **5** and **9**, the quinoxaline rings are oriented toward the sites occupied by basal PEt_3 or *t*-butylisocyanide, a geometry that seems to be sterically disfavored. However, when the substitution happens at the apical positions, as in **2** and **7**, the quinoxaline rings are pushed away from the substituted Fe center to avoid the strong steric repulsion between the quinoxalin rings and phosphine ligands. It is perhaps due to the spatial requirements of the quinoxaline rings, further displacement of CO by tertiary phosphines on the unsubstituted Fe atoms is unfavorable and the second substitution only occurs for the less bulky *t*-Butylisocyanide resulting in the formation of **10**. The

less spatial demand of *t*-Butylisocyanide is also evident from the small distortion away from an eclipsed state of the molecular structures of **9** and **10**, where the average torsional angles between the three non-sulfur substituents on each iron atom are 1.1 and 1.5° respectively. For the more bulky substituents such as PPh_3, the twisting away from the eclipsed state becomes a little more appreciable as the average torsional angle of **7** increases to 7.9° with a maximum of 16.6° associated with P–Fe(1)–Fe(2)–C(5) (Fig. 2(b)). This is especially so in **3** where the average torsional angle is 14.7°, which includes angles of 23.7 and 18.4° between C1–C4 and P2–C2 respectively (Fig. 1(c)). It could be for this reason that **3** is somewhat unstable in solution and readily decomposes during the crystallization process. Despite this asymmetry, the substitution of donor ligands does not change the unrotated nature of the parent complex.

Spectroscopic studies of the protonation of complexes 1–4 by FTIR and ^{1}H NMR

Since protonation of N atoms in the model complexes affects the electrochemical properties of these complexes and their catalytic activity towards hydrogen evolution,[16,20–35] protonation of our complexes in MeCN with HBF_4 were investigated spectroscopically using both FTIR and ^{1}H NMR.

The FTIR spectra of the protonation of **1–4** in MeCN solution with HBF_4 showed similar behavior. Upon addition of one equivalent of acid, the infrared absorption bands of these complexes have no clear shifts. However, after five equivalent acid was added, the carbonyl frequencies in the IR spectra shifted towards higher energy by about 5, 5, 10, and 7 cm^{-1} for **1**, **2**, **3** and **4**, respectively, compared to their corresponding non-protonated forms. These blue shifts clearly indicated that the protonation occurred on the N atoms of quinoxaline rings as they are of the same magnitude as those observed for the protonated model complexes with pyridine or bridgehead N atoms.[14,23,28,47] While **1** requires at least 5 equiv. acid for complete protonation, addition of 3 equiv. acid leads to complete protonation on N atoms for complexes **2–4**. The electron-donating dppm improves the proton binding ability for **2–4**. The protonation could be completely reversed by the addition of 5 equiv. of triethylamine to regenerate the parent complexes.

With regard to the protonated complexes, their ^{1}H NMR spectra show no peak at $\delta < 0$ ppm even at temperatures lower than −70 °C, indicating again that the protonation occurred on the quinoxaline N atoms rather than at the Fe–Fe site to form μ-H complexes. The peaks for the methylene protons of $\mathbf{1}H^+$ appear at 4.72 and 3.65 ppm, shifted to higher magnetic field by 0.49 and 0.25 ppm, respectively, than its parent complex **1**. A similar trend has been observed in the ^{1}H NMR spectra for the protonated species of **2–4**. In addition, a new broad peak at around δ 14.00 emerges in all the ^{1}H-NMR spectra of **1–4** after protonation. These newly-formed signals are tentatively assigned to the NH of protonated quinoxalines. As expected, only slight shifts for the ^{31}P signals of **2–4** were observed when the protonation on N atoms occurred. For example, after protonation, the two doublets in the ^{31}P NMR of **4** shift high-field from 52.4 and 54.1 ppm to 50.7 and 52.5 ppm. Attempts to get single crystals of the protonated species of **1–4** were not successful.

The protonation of complexes **5–10** has also been investigated. The results suggest that these complexes were not stable under acidic conditions.

Electrochemistry of complexes 1–4

Since complexes **5–10** were not stable under acidic conditions, they are not suitable for use as catalysts for hydrogen evolution. Therefore, only the electrochemical properties of complexes **1–4** were investigated with respect to their potential application as catalysts that mimic hydrogenase. The hydrogen evolution reaction catalyzed by the diiron based model hydrogenases is complicated. It involves both electron transfer and protonation reactions. The ability to achieve catalysis is determined by the acid–base properties of the diiron complexes in different redox states. One of the possible reaction mechanisms is summarized in Scheme 4.

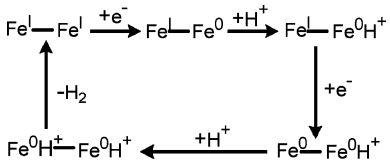

Scheme 4 A possible mechanism for hydrogen evolution catalyzed by a hydrogenase type model diiron complex.

Ideally, if the diiron model complex is to be the catalyst, it should be fully stable during all stages of catalytic reaction. This requires the stability in all three Fe^IFe^I, Fe^IFe^0 and Fe^0Fe^0 redox states both in the presence and absence of acid. From the electrochemical point of view, two one-electron reduction processes involving diiron centers should be chemically reversible. Cyclic voltammetric measurements were therefore, carried out to investigate whether this criterion is satisfied in the case of our diiron complexes.

A cyclic voltammogram of complex **1** obtained at a scan rate of 0.1 V s^{-1} (Fig. 3) is rather complex, exhibiting three reduction and

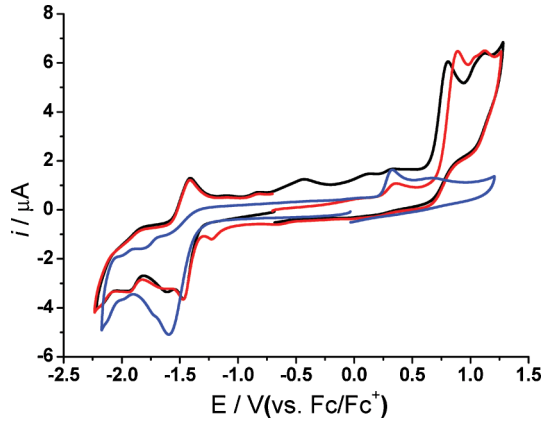

Fig. 3 Cyclic voltammograms of 1 mM **1** in MeCN (0.1 M Bu_4NPF_6) obtained at a 1 mm diameter glassy carbon electrode with a scan rate of 0.1 V s^{-1}. The black curve was obtained by initially scanning the potential in the negative direction. The red curve was obtained by initially scanning the potential in the positive direction. The cyclic voltammogram for 1 mM ligand, 2,3-bis(bromomethyl)quinoxaline (blue curve), was obtained under the same experimental conditions.

two oxidation processes within the solvent/electrolyte potential window. As shown in Fig. 4, the first reduction process has a reversible potential of −1.439 V *vs.* Fc/Fc^+ as calculated from the average of the reduction and oxidation peak potentials (a small shoulder observed at low scan rate is attributed to the protonation of the one-electron reduced form due to the presence of trace water). At moderate scan rates, this is an electrochemically reversible process with a peak-to-peak separation (ΔE_p) of 58 ± 2 mV which is very close to the theoretical value of 57 mV predicted for a reversible one-electron transfer reaction at 25 °C.[48] The fact that this ΔE_p only increases slightly (mostly likely due to uncompensated resistance) and the peak current increases linearly with the square root of the scan rate over the range of 0.05 to 0.5 V s^{-1} also suggests that this process is chemically and electrochemically reversible and diffusion controlled. A diffusion coefficient, D, of 1.23×10^{-5} cm^2 s^{-1} for **1** was calculated based on the Randles–Sevcik relationship,[48]

$$i_p = 0.4463nFA\left(\frac{nFDv}{RT}\right)^{1/2} c^* \quad (1)$$

where i_p is the peak current; n is the number of electron transferred which is assumed to be 1 in this case; F is Faraday's constant; A is the electrode area; v is the scan rate; c^* is the bulk concentration of the electroactive species; R is gas constant and T is temperature (°K). This diffusion coefficient value in MeCN is typical for species having a size similar to complex **1**. Consequently, the first reduction process is assigned to the one-electron reduction of Fe^IFe^I to Fe^IFe^0 as in eqn (2),

$$Fe^IFe^I + e^- \rightleftarrows Fe^IFe^0 \quad (2)$$

All other processes are chemically irreversible with peak potentials of −1.612 and −1.920 V *vs.* Fc/Fc^+ for the two remaining reduction processes, and 0.362, 0.891 and 1.124 V *vs.* Fc/Fc^+ for the three oxidation processes. A cyclic voltammogram obtained from the ligand, 2,3-bis(bromomethyl)quinoxaline, is also included in Fig. 3. *Via* comparison of metal complex and ligand data, the processes found at −1.612 V and 0.362 V *vs.* Fc/Fc^+ are assigned as being ligand based, while the process at −1.920 V most probably represents the reaction scheme, on the basis of the previous studies on the similar compounds.[32,49,50]

$$Fe^IFe^0 + e^- \rightleftarrows Fe^\circ Fe^0 \rightarrow \text{product} \quad (3)$$

Other small peaks (Fig. 3) that follow the irreversible oxidation or reduction processes are attributed to the decomposition products arising from the major processes. A related voltammetric response of complex **1** was obtained in dichloromethane (0.1 M Bu_4NPF_6), but with a reversible potential of −1.610 V *vs.* Fc/Fc^+ for the first one-electron reduction process. Thus, this is a significant thermodynamic effect in changing from acetonitrile where the reversible potential was −1.439 V *vs.* Fc/Fc^+.

Steady state voltammetric experiments were also conducted using a 10 μm diameter gold microdisc electrode in order to provide further understanding of the electrochemical processes. As shown in Fig. 5, two major oxidation processes with half wave potentials of 0.418 and 1.106 V *vs.* Fc/Fc^+ and two major reduction processes with half wave potentials of −1.440 and −1.978 V *vs.* Fc/Fc^+ are observed. A diffusion coefficient of 1.20×10^{-5} cm^2 s^{-1} was calculated from the steady-state diffusion limiting current for the first reduction process from the relationship,

$$i_{ss} = 4nFDrc^* \quad (4)$$

where r is the radius of the electrode and the number of electrons transfer is assumed to be one. The fact that this value of diffusion coefficient obtained agrees well with the one calculated from transient voltammetry (1.23×10^{-5} cm^2 s^{-1}) supports the assumption of a one-electron transfer reaction. The steady-state

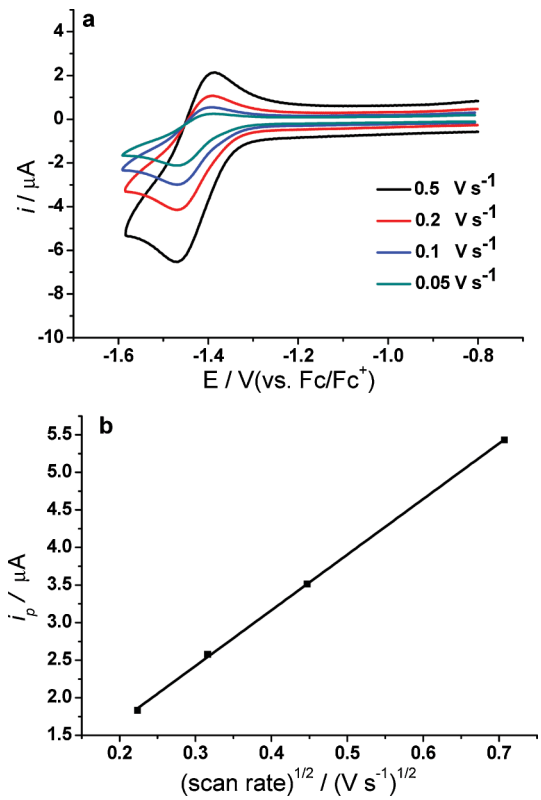

Fig. 4 (a) Cyclic voltmmograms of the first reduction process obtained at scan rates of 0.05, 0.1, 0.2 and 0.5 V s^{-1} with a 1 mm diameter glassy carbon electrode and (b) dependence of the reduction peak current on the square root of scan rate.

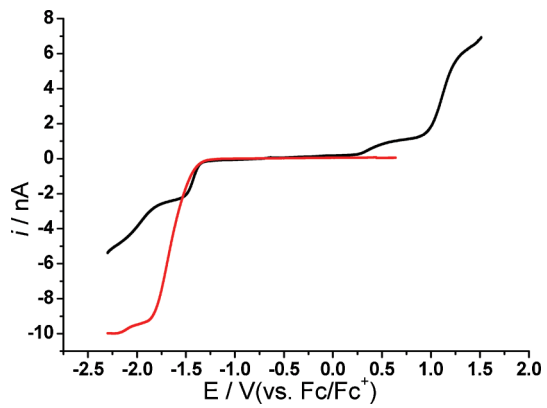

Fig. 5 Steady state voltammograms of 1 mM **1** (black) and ligand, 2,3-bis(bromomethyl) quinoxaline (red) obtained at a 10 μm diameter Au microelectrode. A scan rate of 0.05 V s^{-1} was used.

diffusion controlled limiting current associated with the second reduction process (half wave potential = −1.978 V *vs.* Fc/Fc^+) is comparable to that for the first and is assigned to the reduction scheme given in eqn (3) since the half wave potential of this process is close to the peak potential of −1.92 V obtained from cyclic voltammetry (Fig. 3). The steady-state diffusion controlled limiting current of the first oxidation process (half wave potential = 0.418 V *vs.* Fc/Fc^+) is about half that of the first one-electron reduction process. The response may therefore be associated with an irreversible oxidative dimerization involving complex **1** reacting with the one-electron oxidized form, which is unstable (eqn (5) and 6).

$$Fe^{I}Fe^{I} \rightleftarrows Fe^{II}Fe^{I} + e^{-} \quad (5)$$

$$Fe^{II}Fe^{I} + Fe^{II}Fe^{I} \rightarrow Fe^{II}Fe^{I}\text{-}Fe^{II}Fe^{I} \rightarrow \text{product} \quad (6)$$

The steady-state diffusion controlled limiting current of the second oxidation process (half wave potential = 1.106 V *vs.* Fc/Fc^+) is approximately twice that of the first reduction process. Therefore, this oxidation process could be assigned to a two-electron oxidation process of the product of the first oxidation process. A steady-state voltammogram for the ligand, 2,3-bis(bromomethyl)quinoxaline, reduction process is also included in Fig. 5. Comparison of the steady-state diffusion limiting currents of the ligand and complex **1**, after taking into account the differences in their sizes suggests that the ligand undergoes a two-electron reduction process at a potential similar to the reduction of $Fe^{I}Fe^{I}$. This finding is consistent with those proposed in other electrochemical studies of quinoxaline derivatives.[51]

All of the above findings on the reduction processes are not conducive to anticipating efficient catalysis to form hydrogen and this was not found on the addition of acidic acid and examination of reduction in the acidified medium.

The electrochemistry of other dppm derivatives was also examined in CH_3CN (0.1 M Bu_4NPF_6). The results reveal that even the first reduction of **2–4** is not reversible as was found for **1**. The first reduction peak potentials associated with the $Fe^{I}Fe^{I}$ to unstable $Fe^{0}Fe^{I}$ and then to final product process of complexes **1–4** are −1.468, −1.670, −1.916 and −1.944 V *vs.* Fc/Fc^+, respectively. Thus the first irreversible reductive peaks for **2**, **3** and **4** occur at more negative potentials by 202, 448 and 476 mV, respectively, than that of the parent complex **1**. The electron donor character of dppm would therefore appear to render the reduction of the iron core even more difficult, with di-substitution of dppm exerting additional influence on the redox potential of **1** than the mono-substitution. However, it should be noted that it is not meaningful to directly compare a reduction peak potential for an irreversible process (**2–4**) with that derived from a reversible process (as found for **1**). However, chemical irreversibility of **2–4** is predicted to lead to a positive shift of the reduction peak potential from the reversible case. Therefore, the conclusions on substituent effect reached are probably qualitatively correct.

Again with **2–4**, ideal characteristics for mimicking the behaviors in Scheme 4 or those used by hydrogenase are not available, so prospects for hydrogen catalysis are poor.

Conclusion

A new complex **1** that contains a large conjugated quinoxaline moiety has been prepared as a potential model for hydrogenase active site. Reaction of **1** with dppm yields complexes **2–4** that differ in their dppm coordination modes. In **2**, the dppm is terminally bonded to an iron atom with one phosphorus atom, whereas in **3** or **4**, it attaches to a Fe atom in a dibasal-substituted manner or bridges two Fe atoms in a *cis* basal/basal fashion. CO-substituted derivatives of tertiary phosphines with various electron-donor abilities and t-butylisocyanide derivatives also have been prepared. Electronic effects of the substituted ligands on the structure parameters of the parent complex as well as the electron properties of the diiron site have been studied. In addition, protonation of **1–4** is shown to occur on the quinoxaline N atoms by shifts in the ν_{CO} bands in IR spectra. Electrochemical studies reveal that only **1** can be reduced reversibly *via* a one-electron transfer reaction. However, the electrochemical ease of reduction of the ligand, quinoxaline, and the instability of the two-electron reduced Fe^{0}–Fe^{0} state of complex **1** suggest that this compound does not provide an ideal model of the hydrogenase active site. The even greater instabilities of reduced forms of **2–4** also rule these materials from being efficient hydrogen catalysts.

4. Experimental

Reagents and instruments

All synthetic reactions and operations were carried out under nitrogen atmosphere with standard Schlenk techniques. All solvents were dried and distilled prior to use according to standard methods. Tetrahydrofuran was purified by distillation under N_2 from sodium/benzophenone. MeCN and dichloromethane were distilled from CaH_2 and P_2O_5, respectively, under N_2. The following chemicals were commercially available and used as received: 2,3-bis(bromomethyl)quinoxaline, phosphines, Bu^tNC, $LiEt_3BH$ and $HBF_4{\cdot}OEt_2$. The compounds $[(\mu\text{–}S)_2Fe_2(CO)_6]$ and $[(\mu\text{-}LiS)_2Fe_2(CO)_6]$ were synthesized according to the literature procedure.[52,53] Infrared spectra were recorded with a Spectrum-One FT-IR spectrophotometer. ^1H and ^{31}P NMR spectra were collected on a BRUKER AVANCE III 400 NMR spectrometer. Mass spectra were recorded on a DECAX-30000 LCQ Deca XP instrument. Elemental analyses for C, H, and N were determined using an Elementar Vario EL III elemental analyzer.

Synthesis of complexes 1–10

$[Fe_2\{(\mu\text{-}CH_2S)_2R\}(CO)_6]$ (1). A mixture of 2,3-bis(bromomethyl)quinoxaline (316.01 mg, 1 mmol) and $[(\mu\text{-}LiS)_2Fe_2(CO)_6]$ (357.76 mg, 1 mmol) in THF (20 ml) was stirred 0.5 h under a temperature of −78 °C. After further reaction for 2 h under room temperature, the solvent was removed under vacuum, and the residue was purified by chromatography on silica gel with petroleum ether/ethyl acetate (6 : 1 v/v) as eluent to give **1** as the major product (123 mg, 25%). ^1H NMR ($CDCl_3$): δ 3.40 (d, J = 12.8 Hz, 2H,CCH_2S), 4.29 (d, J = 12.8 Hz, 2H, CCH_2S), 7.26–7.98 (m, 4H, C_6H_4) ppm; IR (CH_3CN): ν(CO) 2079, 2042, 2003 cm^{-1}; MS (ESI): m/z: 499.1 $[M\text{–}H]^-$; Anal. Calcd (%) for $C_{16}H_8Fe_2N_2O_6S_2$: C 38.43, H 1.61, N 5.60. Found: C 38.16, H 1.76, N, 5.58.

[Fe_2{(μ-$CH_2S)_2R$}$(CO)_5$(dppm)] (2). A solution of **1** (50 mg, 0.1 mmol) and Me_3NO (7.5 mg, 1 mmol) in CH_3CN (20 ml) was stirred at room temperature for 15 min. Then, dppm (38.4 mg, 0.1 mmol) was added. After stirring for 2 h, the solvent was removed under reduced pressure and the crude product was purified by chromatography on silica gel with petroleum ether/ethyl acetate (4 : 1 v/v) as eluent to afford **2** as a red solid (180 mg, 77%). ^{1}H NMR ($CDCl_3$): δ 1.26 (s, 2H, PCH_2P), 3.44 (s, 2H, CCH_2S), 3.64 (s, 2H, CCH_2S), 7.15–8.00 (m, 24H, 4Ph, C_6H_4) ppm;^{31}P NMR ($CDCl_3$): δ 55.83 (d, J = 220 Hz), –26.43 (d, J = 216 Hz) ppm; IR (CH_3CN): ν(CO) 2052, 1992, 1943 cm^{-1}; MS (ESI): m/z 856.5; Anal. Calcd (%) for $C_{40}H_{30}Fe_2N_2O_5P_2S_2$: C 56.10, H 3.53, N 3.27. Found: C 56.49, H 3.60, N 3.27.

[Fe_2{(μ-$CH_2S)_2R$}$(CO)_4$(k^2–dppm)] (3) and [Fe_2{(μ-$CH_2S)_2R$}-$(CO)_4$(μ-dppm)] (4). A solution of **1** (100 mg, 0.2 mmol), dppm (76.8 mg, 0.2 mmol), and Me_3NO (30 mg, 0.4 mmol) in toluene (25 ml) was refluxed for 4 h. The solvent was then removed under reduced pressure, and the crude product was purified by chromatography on silica gel with petroleum ether/ethyl acetate (4 : 1 v/v) as eluent. Complexes **3** (35 mg, 21%) and **4** (27 mg, 17%) were isolated. For **3**: ^{1}H NMR ($CDCl_3$): δ 2.07, 2.38 (2 s, 2H, PCH_2P), 3.48 (m, 2H, CCH_2S), 4.24 (m, 2H, CCH_2S), 7.19–7.93 (m, 24H, 4Ph, C_6H_4) ppm; ^{31}P NMR ($CDCl_3$): δ 8.44 (s), 12.43 (s) ppm; IR (CH_3CN): ν(CO) 2023, 1956, 1916 cm^{-1}; MS (ESI): m/z: 827.2 [M – H]$^-$; Anal. Calcd (%) for $C_{39}H_{30}Fe_2N_2O_4P_2S_2$: C 56.49, H 3.62, N 3.38. Found: C 56.69, H 3.54, N 3.48. For **4**: ^{1}H NMR ($CDCl_3$): δ 2.04 (s, 2H, PCH_2P), 3.22–3.74 (m, 2H, CCH_2S), 4.11–4.71 (m, 2H, CCH_2S), 7.12–8.00 (m, 24H, 4Ph, C_6H_4) ppm; ^{31}P NMR ($CDCl_3$): δ 52.42 (d, J = 132 Hz), 54.08(d, J = 132 Hz) ppm; IR (CH_3CN): ν(CO) 1993, 1963, 1929 cm^{-1}; MS (ESI): m/z: 827.0 [M – H]$^-$; Anal. Calcd (%) for $C_{39}H_{30}Fe_2N_2O_4P_2S_2$: C 56.49, H 3.62, N 3.38. Found: C 56.80, H 3.40, N 3.16.

[Fe_2{(μ-$CH_2S)_2R$}$(CO)_5$L] (5: L = PEt_3; 6: PMe_3; 7: PPh_3; 8: PMe_2Ph). In a typical reaction, a solution of **1** (50 mg, 0.1 mmol) and Me_3NO (7.5 mg, 1 mmol) in CH_3CN (20 ml) was stirred at room temperature for 15 min. Then, PMe_3 (10.2 μl, 0.1 mmol) was added. After stirring for 2 h, the solvent was removed under reduced pressure, and the crude product was purified by chromatography on silica gel with petroleum ether/ethyl acetate (4 : 1 v/v) as eluent. Complex **6** was obtained as a red solid (40 mg, 74%). ^{1}H NMR ($CDCl_3$): δ 0.87–1.51 (m, 9H, $3CH_3$), 3.36 (d, J = 12.4 Hz, 2H, CCH_2S), 4.23 (d, J = 12.4 Hz, 2H, CCH_2S). 7.70–7.95 (m, 4H, C_6H_4) ppm; ^{31}P NMR ($CDCl_3$): δ 23.07 (s), 26.09 (s) ppm; IR (CH_3CN): ν(CO) 2044, 1988, 1971, 1930 cm^{-1}; MS (ESI): m/z: 548.9; Anal. Calcd (%) for $C_{18}H_{17}Fe_2N_2O_5PS_2$: C 39.44, H 3.13; N, 5.11. Found: C 39.16, H, 3.11, N 4.85. Complexes **5**, **7** and **8** were synthesized in a similar way as that of **6** by using one equiv of PEt_3, PPh_3 and PMe_2Ph, respectively, instead of PMe_3. For **5** (33 mg, 55%): ^{1}H NMR ($CDCl_3$): δ 1.18–1.23 (m, 15H, $3CH_2CH_3$), 3.40 (d, J = 12.4 Hz, 2H, CCH_2S), 4.26 (d, J = 12.8 Hz, 2H, CCH_2S), 7.26–7.95 (m, 4H, C_6H_4) ppm;^{31}P NMR ($CDCl_3$): δ 56.52 (s), 53.16 (s) ppm; IR (CH_3CN): ν(CO) 2044, 1986, 1970, 1926 cm^{-1}; MS (ESI): m/z: 590.5. Anal. Calcd (%) for $C_{21}H_{23}Fe_2N_2O_5PS_2$: C 42.68, H 3.90, N 4.74. Found: C 42.86, H 3.96, N, 5.00. For **7** (54 mg, 73%): ^{1}H NMR ($CDCl_3$): δ 3.54 (d, 2H, J = 12.4 Hz, CCH_2S), 4.46 (s, 1H, CCH_2S), 7.26–7.89 (m, 19H, 3Ph, C_6H_4) ppm;^{31}P NMR ($CDCl_3$): δ 64.21 (s), 64.14 (s) ppm; IR (CH_2Cl_2): ν(CO) 2051, 1993, 1939 cm^{-1}; MS (ESI): m/z: 734.5. Anal. Calcd (%) for $C_{33}H_{23}Fe_2N_2O_5PS_2$: C 53.91, H 3.13, N 3.81. Found: C 54.13, H 3.26, N 3.72. For **8** (38 mg, 63%): ^{1}H NMR ($CDCl_3$): δ 0.88–2.01 (m, 6H, $2CH_3$), 3.35 (d, J = 10.8 Hz, 2H, CCH_2S), 4.20 (s, 2H, CCH_2S), 7.26–7.94 (m, 9H, Ph, C_6H_4) ppm;^{31}P NMR ($CDCl_3$): δ 33.65(s), 30.19(s) ppm; IR (CH_2Cl_2): ν(CO) 2046, 1989, 1968, 1931 cm^{-1}; MS (ESI): m/z: 610.6. Calcd (%) for $C_{23}H_{19}Fe_2N_2O_5PS_2$: C 45.27, H 3.14, N 4.59. Found: C 45.39, H 3.10, N 4.49.

[Fe_2{(μ-$CH_2S)_2R$}$(CO)_5$(Bu^{t}NC)] (9) and [Fe_2{(μ-$CH_2S)_2R$}-$(CO)_4$(Bu^{t}NC)$_2$] (10). Complexes **9** and **10** were synthesized in a similar manner to **5** except that one or two equiv of Bu^{t}NC, were employed. For **9** (38 mg, 63%): ^{1}H NMR ($CDCl_3$): δ 1.34, 1.37 (2 s, 9H, $3CH_3$), 3.31 (m, 2H, CCH_2S), 4.13 (m, 2H, CCH_2S), 7.26–7.96 (m, 4H, C_6H_4) ppm; IR (CH_3CN): ν(CO) 2048, 2007, 1978, 1958 cm^{-1}; MS (ESI): m/z: 556.1 [M+H]$^+$; Anal. Calcd (%) for $C_{20}H_{17}Fe_2N_3O_5S_2$: C 43.24, H 3.06, N 7.57. Found: C 43.47, H 3.43, N, 7.82. For **10** (43 mg, 70%): ^{1}H NMR ($CDCl_3$): δ 1.27–1.61 (m, 18H, $6CH_3$), 3.23(d, J = 9.6 Hz, 2H, CCH_2S), 4.05 (d, J = 11.6 Hz, CCH_2S), 7.26–7.95 (m, 4H, C_6H_4) ppm; IR (CH_3CN): ν(CO) 2005, 1977, 1946 cm^{-1}; MS (ESI): m/z: 610.7; Anal. Calcd (%) for $C_{24}H_{26}Fe_2N_4O_4S_2$: C 47.23, H 4.29, N 9.18. Found: C 47.55, H 4.03, N 9.24.

Crystal structure determination of complexes 1–5, 7, 9 and 10

X-ray diffraction data were collected on a Rigaku diffractometer with a Mercury CCD area detector (Mo-Kα; λ = 0.71073 Å) at 293(2) K. Empirical absorption corrections were applied to the data using the CrystalClear program.[54] The structures were solved by the direct method and refined by the full-matrix least-squares on F^2 using the SHELXTL-97 program.[55] All the non-hydrogen atoms were refined anisotropically. The hydrogen atoms were all treated by geometrical positions. Crystallographic data and other pertinent information for **1–5**, **7**, **9** and **10** are summarized in Tables 2 and 3 .

Electrochemistry

Electrochemical measurements were carried out using a CHI 700 Electrochemical Workstation (CH Instruments, Austin, Texas, USA). Cyclic voltammetric measurements were performed in MeCN containing 0.1 M Bu_4NPF_6 as the supporting electrolyte with a glassy carbon electrode (1 mm or 3 mm diameter) as the working electrode and platinum wires as both the quasi-reference and counter electrodes. Steady state voltammograms were obtained with a gold microelectrode (10 μm diameter) as the working electrode and platinum wires again as both the quasi-reference and counter electrodes. The Pt quasi-potential scale was then calibrated against the Fc/Fc^+ couple and potentials are reported *versus* this reference system. All electrochemical experiments were carried out at 25 ± 2 °C in a dry box under N_2 atmosphere.

Appendix A. Supporting information

CCDC 816112–816119 contains supplementary crystallographic data for the complexes **1–5**, **7**, **9** and **10**. These data can be obtained free of charge from the Cambridge Crystallographic Data Center *via* http://www.ccdc.cam.ac.uk/data_request/cif.

Table 2 Crystal data and structure refinement details for **1–4**

Complex	**1**·0.5CH_2Cl_2	**2**	**3**·CH_2Cl_2	**4**·2CH_2Cl_2
Mol. formula	$C_{16.5}H_9Cl\ Fe_2N_2O_6S_2$	$C_{40}H_{30}Fe_2N_2\ O_5P_2S_2$	$C_{40}H_{32}Cl_2\ Fe_2N_2O_4P_2S_2$	$C_{41}H_{34}Cl_4Fe_2\ N_2O_4P_2S_2$
FW	542.53	856.42	913.34	998.26
Cryst. syst.	Triclinic	Triclinic	Triclinic	Triclinic
Space group	$P\bar{1}$	$P\bar{1}$	$P\bar{1}$	$P\bar{1}$
a/Å	6.801(2)	9.2471(6)	10.199(7)	10.518(6)
b/Å	11.254(4)	12.8115(8)	13.712(9)	11.149(6)
c/Å	13.330(5)	16.3337(10)	14.582(9)	18.267(11)
α (°)	89.908(12)	98.516(4)	92.981(8)	86.244(12)
β (°)	81.324(10)	95.659(2)	91.827(7)	88.721(11)
γ (°)	77.667(10)	96.527(3)	100.728(13)	87.302(13)
V/Å^3	984.7(6)	1888.1(2)	1999(2)	2135(2)
Z	2	2	2	2
D_c/g cm^{-3}	1.830	1.506	1.517	1.553
μ/mm^{-1}	1.859	1.011	1.087	1.147
F(000)	542	876	932	1016
Rflns collected	7453	14834	11750	14946
Rflns unique	4329	8510	6216	6616
Parameters	290	594	487	514
R_1	0.0463	0.0451	0.0500	0.0748
wR_2	0.1376	0.1075	0.1364	0.1936
GOF	1.040	1.005	1.026	1.087

Table 3 Crystal data and structure refinement details for complexes **5**, **7**, **9** and **10**

Complex	**5**	**7**	**9**·CH_2Cl_2·H_2O	**10**
Mol. formula	$C_{21}H_{23}Fe_2N_2O_5PS_2$	$C_{33}H_{23}Fe_2\ N_2O_5PS_2$	$C_{21}H_{21}Cl_2Fe_2\ N_3O_6S_2$	$C_{24}H_{26}Fe_2\ N_4O_4S_2$
FW	590.20	734.32	658.13	610.31
Cryst. syst.	Triclinic	Triclinic	Triclinic	Triclinic
Space group	$P\bar{1}$	$P\bar{1}$	$P\bar{1}$	$P\bar{1}$
a/Å	6.934(4)	9.3335(0)	9.174(4)	10.390(3)
b/Å	12.827(7)	12.73310(10)	11.761(6)	11.082(3)
c/Å	13.646(7)	14.2960(2)	13.765(7)	13.014(4)
α (°)	87.864(11)	93.811(11)	89.067(15)	85.726(8)
β (°)	86.760(12)	105.134(7)	81.459(14)	86.282(7)
γ (°)	81.660(12)	109.359(7)	72.711(10)	68.586(6)
V/Å^3	1198.5(11)	1525.35(2)	1401.7(12)	1389.9(6)
Z	2	2	2	2
D_c/g cm^{-3}	1.636	1.599	1.559	1.458
μ/mm^{-1}	1.487	1.187	1.414	1.230
F(000)	604	748	668	628
Rflns collected	9427	11926	10801	11001
Rflns unique	5387	6846	6235	6271
Parameters	298	406	325	325
R_1	0.0424	0.0373	0.0592	0.0451
wR_2	0.1327	0.0913	0.1602	0.1064
GOF	1.051	1.065	1.007	1.003

Acknowledgements

This work was supported by the grants from the State Key Laboratory of Structural Chemistry, Fujian Institute of Research on the Structure of Matter, Chinese Academy of Sciences, National Basic Research Program of China (973 Program, 2007CB815306), and the National Natural Science Foundation of China (20733003). JZ and AMB also would like to thank the Australian Research Council for financial support.

References

1 R. Cammack, *Nature*, 1999, **397**, 214–215.
2 H. L. Karunadasa, C. J. Chang and R. J. Long, *Nature*, 2010, **464**, 1329–1333.
3 M. Y. Darensbourg, E. J. Lyon, X. Zhao and I. P. Georgakaki, *Proc. Natl. Acad. Sci. U. S. A.*, 2003, **100**, 3683–3688.
4 D. J. Evans and C. J. Pickett, *Chem. Soc. Rev.*, 2003, **32**, 268–275.
5 J. Alper, *Science*, 2003, **299**, 1686–1687.
6 J. L. Dempsey, B. S. Brunschwig, J. R. Winkler and H. B. Gray, *Acc. Chem. Res.*, 2009, **42**, 1995–2004.
7 Y. Nicolet, C. Piras, P. Legrand, C. E. Hatchikian and J. C. Fontecilla-Camps, *Structure*, 1999, **7**, 13–23.
8 J. W. Peters, W. N. Lanzilotta, B. J. Lemon and L. C. Seefeldt, *Science*, 1998, **282**, 1853–1858.
9 Y. Nicolet, B. J. Lemon, J. C. Fontecilla-Camps and J. W. Peters, *Trends Biochem. Sci.*, 2000, **25**, 138–143.
10 E. J. Lyon, I. P. Georgakaki, J. H. Reibenspies and M. Y. Darensbourg, *Angew. Chem., Int. Ed.*, 1999, **38**, 3178–3180.
11 F. Gloaguen, J. D. Lawrence, M. Schmidt, S. R. Wilson and T. B. Rauchfuss, *J. Am. Chem. Soc.*, 2001, **123**, 12518–12527.
12 J. L. Nehring and D. M. Heinekey, *Inorg. Chem.*, 2003, **42**, 4288–4292.
13 J. W. Tye, J. Lee, H. W. Wang, R. Mejia-Rodriguez, J. H. Reibenspies, B. Michael and M. Y. Darensbourg, *Inorg. Chem.*, 2005, **44**, 5550–5552.
14 P. Li, M. Wang, C. He, G. Li, X. Liu, C. Chen, B. kermark and L. Sun, *Eur. J. Inorg. Chem.*, 2005, 2506–2513.

15 D. Morvan, J. F. Capon, F. Gloaguen, A. Le Goff, M. Marchivie, F. Michaud, P. Schollhammer, J. Talarmin, J. J. Yaouanc and R. Pichon, *Organometallics*, 2007, **26**, 2042–2052.
16 W. Gao, J. Ekstrm, J. Liu, C. Chen, L. Eriksson, L. Weng, B. kermark and L. Sun, *Inorg. Chem.*, 2007, **46**, 1981–1991.
17 M. L. Singleton, N. Bhuvanesh, J. H. Reibenspies and M. Y. Darensbourg, *Angew. Chem., Int. Ed.*, 2008, **47**, 9492–9495.
18 L. C. Song, C. G. Li, J. Gao, B. S. Yin, X. Luo, X. G. Zhang, H. L. Bao and Q. M. Hu, *Inorg. Chem.*, 2008, **47**, 4545–4553.
19 P. Li, M. Wang, L. Chen, J. Liu, Z. Zhao and L. Sun, *Dalton Trans.*, 2009, 1919–1926.
20 J. D. Lawrence, H. Li, T. B. Rauchfuss, M. Bénard and M. M. Rohmer, *Angew. Chem., Int. Ed.*, 2001, **40**, 1768–1771.
21 J. D. Lawrence, H. Li and T. B. Rauchfuss, *Chem. Commun.*, 2001, 1482–1493.
22 W. Gao, J. Liu, C. Ma, L. Weng, K. Jin, C. Chen, B. Akermark and L. Sun, *Inorg. Chim. Acta*, 2006, **359**, 1071–1080.
23 W. Gao, J. Liu, B. Akermark and L. Sun, *J. Organomet. Chem.*, 2007, **692**, 1579–1583.
24 J. F. Capon, S. Ezzaher, F. Gloaguen, F. Y. Pétillon, P. Schollhammer, J. Talarmin, T. J. Davin, J. E. McGrady and K. W. Muir, *New J. Chem.*, 2007, **31**, 2052–2064.
25 Y. Si, C. Ma, M. Hu, H. Chen, C. Chen and Q. Liu, *New J. Chem.*, 2007, **31**, 1448–1454.
26 S. Ott, M. Kritikos, B. kermark, L. Sun and R. Lomoth, *Angew. Chem., Int. Ed.*, 2004, **43**, 1006–1009.
27 T. Liu, M. Wang, Z. Shi, H. Cui, W. Dong, J. Chen, B. kermark and L. Sun, *Chem. Eur. J.*, 2004, **10**, 4474–4479.
28 L. Schwartz, G. Eilers, L. Eriksson, A. Gogoll, R. Lomoth and S. Ott, *Chem. Commun.*, 2006, 520–522.
29 L. C. Song, J. H. Ge, X. G. Zhang, Y. Liu and Q. M. Hu, *Eur. J. Inorg. Chem.*, 2006, 3204–3210.
30 L. C. Song, H. T. Wang, J. H. Ge, S. Z. Mei, J. Gao, L. X. Wang, B. Gai, L. Q. Zhao, J. Yan and Y. Z. Wang, *Organometallics*, 2008, **27**, 1409–1416.
31 W. G. Wang, H. Y. Wang, G. Si, C. H. Tung and L. Z. Wu, *Dalton Trans.*, 2009, 2712–2720.
32 P. Li, M. Wang, J. Pan, L. Chen, N. Wang and L. Sun, *J. Inorg. Biochem.*, 2008, **102**, 952–959.
33 S. Jiang, J. Liu, Y. Shi, Z. Wang, B. kermark and L. Sun, *Dalton Trans.*, 2007, 896–902.
34 F. Xu, C. Tard, X. Wang, S. K. Ibrahim, D. L. Hughes, W. Zhong, X. Zeng, Q. Luo, X. Liu and C. J. Pickett, *Chem. Commun.*, 2008, 606–608.
35 S. Jiang, J. Liu, Y. Shi, Z. Wang, B. Akermark and L. Sun, *Polyhedron*, 2007, **26**, 1499–1504.
36 G. Eilers, L. Schwartz, M. Stein, G. Zampella, L. de Gioia, S. Ott and R. Lomoth, *Chem.–Eur. J.*, 2007, **13**, 7075–7084.
37 R. D. Adams and S. Miao, *Inorg. Chem.*, 2004, **43**, 8414–8426.
38 L. Schwartz, P. S. Singh, L. Eriksson, R. Lomoth and S. Ott, *C. R. Chim.*, 2008, **11**, 875–889.
39 L. Schwartz, L. Eriksson, R. Lomoth, F. Teixidor, C. Vias and S. Ott, *Dalton Trans.*, 2008, 2379–2381.
40 C. M. Thomas, O. Rüdiger, T. Liu, C. E. Carson, B. Michael and M. Y. Darensbourg, *Organometallics*, 2007, **26**, 3976–3984.
41 F. I. Adam, G. Hogarth and I. Richards, *J. Organomet. Chem.*, 2007, **692**, 3957–3968.
42 X. Zhao, I. P. Georgakaki, M. L. Miller, R. Mejia-Rodriguez, C. Y. Chiang and M. Y. Darensbourg, *Inorg. Chem.*, 2002, **41**, 3917–3928.
43 J. A. Cabeza, M. A. Martínez-García, V. Riera, D. Ardura and S. Garcia-Granda, *Organometallics*, 1998, **17**, 1471–1477.
44 M. M. Hasan, M. B. Hursthouse, S. E. Kabir and K. Malik, *Polyhedron*, 2001, **20**, 97–101.
45 L. C. Song, X. Luo, Y. Z. Wang, B. Gai and Q. M. Hu, *J. Organomet. Chem.*, 2009, **694**, 103–112.
46 J. Hou, X. Peng, J. Liu, Y. Gao, X. Zhao, S. Gao and K. Han, *Eur. J. Inorg. Chem.*, 2006, **22**, 4679–4686.
47 J. L. Stanley, Z. M. Heiden, T. B. Rauchfuss, S. R. Wilson, L. De Gioia and G. Zampella, *Organometallics*, 2007, **26**, 1907–1911.
48 A. J. Bard and L. R. Faulkner, *Electrochemical methods: fundamentals and applications*, A1bazaar, 2006.
49 R. Mejia-Rodriguez, D. Chong, J. H. Reibenspies, M. P. Soriaga and M. Y. Darensbourg, *J. Am. Chem. Soc.*, 2004, **126**, 12004–12014.
50 S. J. Borg, T. Behrsing, P. Stephen, M. Razavet, X. Liu and C. J. Pickett, *J. Am. Chem. Soc.*, 2004, **126**, 16988–16999.
51 J. Armand, C. Bellec, L. Boulares, P. Chaquin, D. Masure and J. Pinson, *J. Org. Chem.*, 1991, **56**, 4840–4845.
52 L. E. Bogan, *J. Organomet. Chem.*, 1983, **250**, 429–438.
53 D. Seyferth, G. B. Womack, R. S. Henderson, M. Cowie and B. W. Hames, *Organometallics*, 1986, **5**, 1568–1575.
54 G. M. Sheldrick, *SADABS*, University of Göttingen: Göttingen, Germany, 1996.
55 G. Sheldrick, *SHELXTL. Version 5.1*, Siemens Analytical X-ray Instruments Inc., Madison, Wisconsin, USA, 1994.